Impacts of Climate Change on the Subduction of Mode and Intermediate Water Masses in the Southern Ocean

STEPHANIE M. DOWNES

Institute of Antarctic and Southern Ocean Studies, and Antarctic Climate and Ecosystems Cooperative Research Centre, Hobart, Tasmania, Australia

NATHANIEL L. BINDOFF

Centre for Australian Weather and Climate Research, and Institute of Antarctic and Southern Ocean Studies, and Antarctic Climate and Ecosystems Cooperative Research Centre, Hobart, Tasmania, Australia

STEPHEN R. RINTOUL

Centre for Australian Weather and Climate Research, and Antarctic Climate and Ecosystems Cooperative Research Centre, Hobart, Tasmania, Australia

(Manuscript received 2 June 2008, in final form 3 December 2008)

ABSTRACT

Changes in the temperature, salinity, and subduction of Subantarctic Mode Water (SAMW) and Antarctic Intermediate Water (AAIW) between the 1950s and 2090s are diagnosed using the CSIRO Mark version 3.5 (Mk3.5) climate system model Caps under a CO_2 forcing that reaches 860 ppm by the year 2100. These Southern Ocean upper-limb water masses ventilate the ocean interior, and changes in their properties have been related to climate change in numerous studies. Over time, the authors follow the low potential vorticity and salinity minimum layers describing SAMW and AAIW and find that the water column in the 2090s shifts to lighter densities by approximately 0.2 kg m^{-3}. The model projects a reduction in the SAMW and AAIW annual mean subduction rates as a result of a combination of a shallower mixed layer, increased potential vorticity at the base of the mixed layer, and a net buoyancy gain. There is little change in the projected total volume of SAMW transported into the ocean interior via the subduction process; however, the authors find a significant decrease in the subduction of AAIW. The authors find overall that increases in the air–sea surface heat and freshwater fluxes mainly control the reduction in the mean loss of the SAMW and AAIW surface buoyancy flux when compared with the effect of changes supplied by Ekman transport because of increased zonal wind stress. In the A2 scenario, there are cooling and freshening on neutral density surfaces less than 27.3 kg m^{-3} in response to the warming and freshening observed at the ocean's surface. The model projects deepening of density surfaces due to southward shifts in the outcrop regions and the downward displacement of these surfaces north of 45°S. The volume transport across 32°S is predicted to decrease in all three basins, with southward transport of SAMW and AAIW decreasing by up to 1.2 and 2.0 Sv (1 Sv $\equiv 10^6$ m^3 s^{-1}), respectively, in the Indian Ocean. These projected reductions in the subduction and transport of mode and intermediate water masses in the CSIRO Mk3.5 model could potentially decrease the absorption and storage of CO_2 in the Southern Ocean.

1. Introduction

The Southern Ocean water masses play an important role in the global climate system by storing heat, freshwater, and dissolved gases and absorbing a large portion of the global anthropogenic CO_2 (Sarmiento et al. 1998; Sabine et al. 1999). Subantarctic Mode Water (SAMW) and Antarctic Intermediate Water (AAIW) make up the upper limb of the Southern Ocean's thermohaline circulation and can extend as far as 30°N (Drijfhout et al. 2005), ventilating the subtropical gyres and transferring the properties of the ocean's surface into its interior (Sallée et al. 2006). SAMW spreads mainly in two directions: first, spreading into the Indian subtropical gyre and second, deepening and becoming cooler and denser as it moves along the Antarctic Circumpolar

Corresponding author address: Stephanie Downes, AOS Program, Princeton University, 300 Forrestal Road, Sayre Hall, Princeton, NJ 08544.
E-mail: s.downes@princeton.edu

DOI: 10.1175/2008JCLI2653.1

Current (ACC) and contributes to the South Pacific subtropical gyre and to the formation of AAIW in the southeast Pacific. The cold, low-salinity AAIW predominantly forms in the southeast Pacific near the Subantarctic Front (SAF), circulating to the north and west via the Pacific subtropical gyre and eastward along the ACC (Santoso and England 2004). SAMW has been used to trace anthropogenic signals of climate change (Banks et al. 2002), and both SAMW and AAIW absorb large quantities of anthropogenic CO_2, particularly because of a combination of strong wind stress and an initially weak anthropogenic CO_2 capacity (Sabine et al. 2004). Changes in the properties of mode and intermediate water masses have the potential to alter the uptake and storage of CO_2 in the Southern Ocean.

Increased stratification in the Southern Ocean would ultimately lead to reduced vertical transport of carbon through decreased mixing and convective overturning (Sarmiento et al. 1998; Sabine et al. 1999). The focus of this study is to link changes at the ocean surface with those occurring in the interior. We analyze subduction rates and changes in mode and intermediate water mass properties under increasing CO_2 forcing, using the Commonwealth Scientific and Industrial Research Organisation Mark version 3.5 (CSIRO Mk3.5) climate system model. In particular we compare the decadal means from the 1950s (1951–60) and 2090s (2091–2100), as SAMW and AAIW have been found to circulate on time scales between 5 and 25 yr (Fine et al. 2008). The 1950s means are calculated using the twentieth-century mean climate runs from the Intergovernmental Panel on Climate Change (IPCC) Fourth Assessment Report (AR4) and the 2090s data are from the A2 scenario, in which atmospheric CO_2 reaches 860 ppm by the year 2100. We note that output from the CSIRO Mk3.5 model is not presented in the AR4; however, it is an upgraded version of the CSIRO Mk3.0 model and now part of the IPCC model suite (available online at http://www-pcmdi.llnl.gov/). Our analysis showed that, on decadal time scales for the zonally averaged quantities, the changes from the control in thermodynamic variables, such as density, grow steadily and with an increasing rate during the twenty-first century.

Difficulties in separating the anthropogenic changes from natural variations using observations arise from incomplete temporal and spatial coverage of hydrographic observations across the Southern Ocean (Bryden et al. 2003; Murray et al. 2007). However, temperature and salinity (S) changes in SAMW and AAIW have been attributed to air–sea fluxes (ASFs) of heat and freshwater (Bindoff and McDougall 2000; Banks and Bindoff 2003; Murray et al. 2007) and to the Ekman transport of heat and freshwater generated by changes in wind stress (Rintoul and England 2002; Sallée et al. 2006), with the relative importance of these processes varying regionally. Late-twentieth-century temperature in the Southern Ocean increased by 0.17°C over a 30-yr period (1950s–80s), between depth levels 700 and 1100 m, at a higher rate than the global ocean, and, paradoxically, these changes are comparable in magnitude to the observed atmospheric temperatures (Gille 2002). Freshening of AAIW and Upper Circumpolar Deep Water (UCDW) of about 0.02 psu has been observed in the South Atlantic since the 1950s (Curry et al. 2003) and freshening of between 0.02 and 0.1 psu has been observed in the Indian Ocean at AAIW and SAMW densities (Aoki et al. 2005). Density surfaces at midlatitudes in the Southern Hemisphere have deepened since the 1950s (Wong et al. 1999), and this has been associated with cooling and freshening of SAMW and AAIW density surfaces around 50°S (Bindoff and McDougall 2000). The observed cooling and freshening signals appear strongest in SAMW, equatorward of the SAF, around the 27.0 kg m^{-3} density surface (Rintoul and England 2002; Aoki et al. 2005). These observations indicate that heat and freshwater changes at the ocean surface are the primary source of changes in SAMW and AAIW properties.

Water masses ventilate the ocean's interior through the process of subduction, whereby the deepening of the winter mixed layer (WML) and changes in the surface buoyancy flux lead to convective overturning, allowing fluid to pass irreversibly into the permanent thermocline. Recent studies, such as Marshall et al. (1993, hereafter referred to as MNW) and Spall et al. (2000), calculate water mass subduction kinematically, using the vertical and horizontal velocities combined with the mixed layer depth. The application of this method has focused mainly on midlatitude regions in the North Atlantic in which the annual subduction rate has been observed to range between 50 and 100 m yr^{-1} on the equatorward side of the North Atlantic subtropical gyre. In this region, the heat and freshwater fluxes, rather than the Ekman transport, largely determine the subduction rate of fluid into the permanent thermocline (MNW). Karstensen and Quadfasel (2002) and Goes et al. (2008) diagnosed the annual mean subduction rate (for densities lighter than 27.3 kg m^{-3}) at a similar magnitude in the Southern Hemisphere. We apply the methods of MNW to analyze long-term changes in water mass subduction rates on neutral density surfaces (γ^n) and to determine the contribution of heat, freshwater fluxes, and Ekman transport on the changes in the net buoyancy flux driving subduction in the CSIRO Mk3.5 simulation.

The goal of this paper is to diagnose the impact of future climate change on SAMW and AAIW, and our study is divided as follows: Section 2 outlines the climate model we used and the concepts governing our analysis. Section 3 describes the changes in temperature and salinity on neutral density surfaces and the rates of volume transport and subduction. Section 4 discusses the relationship between changes in the surface forcing and changes in the ocean's interior.

2. Data and methods

a. The CSIRO Mk3.5 climate system model

We analyzed output from the CSIRO Mk3.5 climate system model, which is a fully coupled atmosphere, ocean, and sea ice model. Selected features are briefly described here and the reader should refer to Gordon et al. (2002) for a more detailed discussion of the model. The three-dimensional ocean general circulation component is the Geophysical Fluid Dynamics Laboratory (GFDL) Modular Ocean Model version 2.2 (MOM2.2) code (Pacanowski 1996). An Arakawa B grid is used with a resolution of approximately 0.84°, zonally, and 1.875°, meridionally, spaced evenly over the globe. The 31 vertical layers in the model have a resolution that ranges from 5 m at the surface to 400 m for depths greater than 2 km, and the ocean surface is bounded by a rigid lid. The surface heat and freshwater fluxes as well as the wind stresses are from the atmospheric component of the model. The ocean component uses the ''quicker'' tracer advective scheme—a modification of the quick scheme of Leonard (1979). The model includes the Gent and McWilliams (1990) isopycnal mixing scheme and an adiabatic eddy-induced transport (Visbeck et al. 1997). Further, the ACC transport through the Drake Passage is 145 Sv (1 Sv $\equiv 10^6$ m^3 s^{-1}) at the end of the twentieth century (using the preindustrial run), which falls within 10% of the observed 135 Sv in Cunningham et al. (2003). The depth of density surfaces agrees well with observations in the SAMW formation region in the southeast Indian Ocean (Orsi and Whitworth 2007) and is approximately 150 m deeper than observations for densities greater than 27.0 kg m^{-3} across the Pacific Ocean (Talley 2007). The position of the salinity minimum (around 900 m in the Indian Ocean and 650 m in the Pacific Ocean) is similar to both observations (Orsi and Whitworth 2007) as well as other IPCC models (Sloyan and Kamenkovich 2007), making the CSIRO Mk3.5 model appropriate for analysis of changes in SAMW and AAIW.

The 1950s model SAMW and AAIW formation regions can be identified by the deep winter mixed layers of over 400 m just north of the zero wind stress curl in the southeast Indian and southeast Pacific Oceans, respectively (Fig. 1a). The model projects that the mixed layer depth decreases in the 2090s (Fig. 1b) and significant shoaling by up to 200 m is present in the SAMW and AAIW formation regions (Fig. 1c). The impacts of the mixed layer spatial gradient on the subduction rate will be discussed later in the paper. We calculate the mixed layer depth using the criterion $|\rho_m - \rho_s| \leq 0.03$ kg m^{-3}, where ρ_m and ρ_s are the densities at the base of the mixed layer and at the ocean's surface, respectively. Sallée et al. (2006) compared three different methods of defining the mixed layer depth and found that the above criterion was the most appropriate for analyzing SAMW and de Boyer Montégut et al. (2004) concluded this to be the best global mixed layer criterion. The model maximum winter mixed layer depth is about 500 m, which compares well with other studies (e.g., Banks et al. 2002; Sallée et al. 2006). The majority of studies estimating the Southern Hemisphere subduction rates use a mixed layer criterion in which the surface and mixed layer base densities differ by no more than 0.125 kg m^{-3} (Karstensen 2004; Marshall et al. 1993; Huang and Qiu 1998). This large criterion is based on the subtropical North Atlantic mode waters (de Boyer Montégut et al. 2004); however, we used the smaller criterion of $|\rho_m - \rho_s| \leq 0.03$ kg m^{-3}, which has been found to be the optimal measure of the mixed layer depth in the Southern Ocean (Sallée et al. 2006; de Boyer Montégut et al. 2004). Using a mixed layer depth criterion of $|\rho_m - \rho_s| \leq 0.125$ kg m^{-3} produces SAMW and AAIW winter mixed layers in excess of 600 m, which is greater than observed.

Changes in mode and intermediate water masses have been found to occur over both interannual (Rintoul and England 2002) and decadal (Johnson and Orsi 1997; Aoki et al. 2003; Murray et al. 2007) time scales. Here, we focus on the long-term changes between the 1950s and 2090s by comparing differences between the means over each decade. SAMW is defined by a deep winter mixed layer and is low in large-scale potential vorticity (Rintoul and England 2002; Sallée et al. 2006), which corresponds to the widely spaced isopycnals in Fig. 2. The combination of SAMW water mass properties and cold, fresh waters transported along the ACC contributes to the temperature and salinity properties of AAIW in the Pacific and Atlantic. We found the model salinity minimum of AAIW was best developed in the southeast Pacific Ocean, ranging between 33.75 and 34.25 psu in the 1950s and 2090s. The locations of the AAIW salinity minimum in the southeast Pacific Ocean, the SAMW potential vorticity minimum in the southeast Indian Ocean, and the regions of largest mixed layer

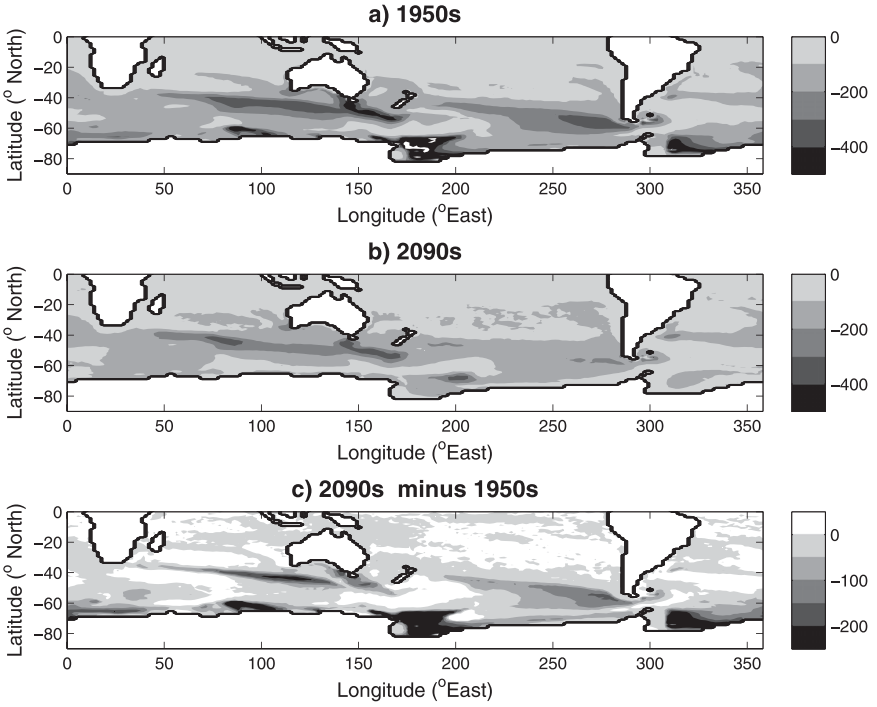

FIG. 1. Southern Hemisphere winter mixed layer depth (m) for the (a) 1950s and (b) 2090s decadal periods and (c) their difference (2090s minus 1950s). Note the different depth shadebar range in the last plot.

depth remain fixed over time in the model. However, the densities at the base of the mixed layer, and hence the densities of SAMW and AAIW, change significantly between the 1950s and 2090s (by about 0.2 kg m^{-3}) because of altered surface fluxes. To quantitatively assess the changes between the two decadal periods, we have defined density classes associated with SAMW and AAIW in each basin for each period (Table 1), using low potential vorticity (to identify SAMW) and the salinity minimum (to identify AAIW). The SAMW and AAIW densities are projected to decrease by approximately 0.3 kg m^{-3} in the 2090s (Fig. 2b) in the Indian and Pacific basins compared to the 1950s (Fig. 2a); smaller changes ($\sim$0.1 kg m^{-3}) occur in the Atlantic basin (Table 1).

b. *Changes on neutral density surfaces*

We analyze water mass changes in the Southern Ocean's interior on neutral density surfaces (Jackett and McDougall 1997) rather than on isobars. Throughout this paper we use neutral density surfaces and refer to them as density surfaces. Furthermore, potential temperature (θ) is referred to as temperature and salinity is S. The CSIRO Mk3.5 climate model is able to simulate climate without the use of flux adjustments; however, it does contain climate drift throughout the water column (Gordon et al. 2002). Significant climate drift is present in temperature and salinity variables when comparing the preindustrial control run (PIcntrl; atmospheric CO_2 set at 290 ppm) and the twentieth-century mean climate (20C3M), and this drift tends to increase into the twenty-first century. The internal variability of either the control or the A2 scenario for zonal averaged quantities is typically very small relative to the change from decade to decade and, more importantly, relative to the difference between the control and the twentieth century and A2 scenarios. We estimate the model drift as the difference between the decadal means in the control experiment

$$\text{DRIFT} = (\text{PIcntrl}_{2090s} - \text{PIcntrl}_{1950s}), \qquad (1)$$

which is then removed from the model projected trend (A2) for our analysis of temperature and salinity changes in the ocean interior. We do not subtract the drift estimate for other variables (e.g., the velocities) because the mean drift is small in the model. The CSIRO Mk3.5 model upper-ocean temperature and salinity drift [Eq. (1)] is a maximum of 0.4°C and 0.1 psu (over the 150-yr period) in the SAMW and AAIW formation regions, which is less than the magnitudes of drift found over a shorter time scale (110 yr) in some of the IPCC models performing a good simulation of SAMW and AAIW

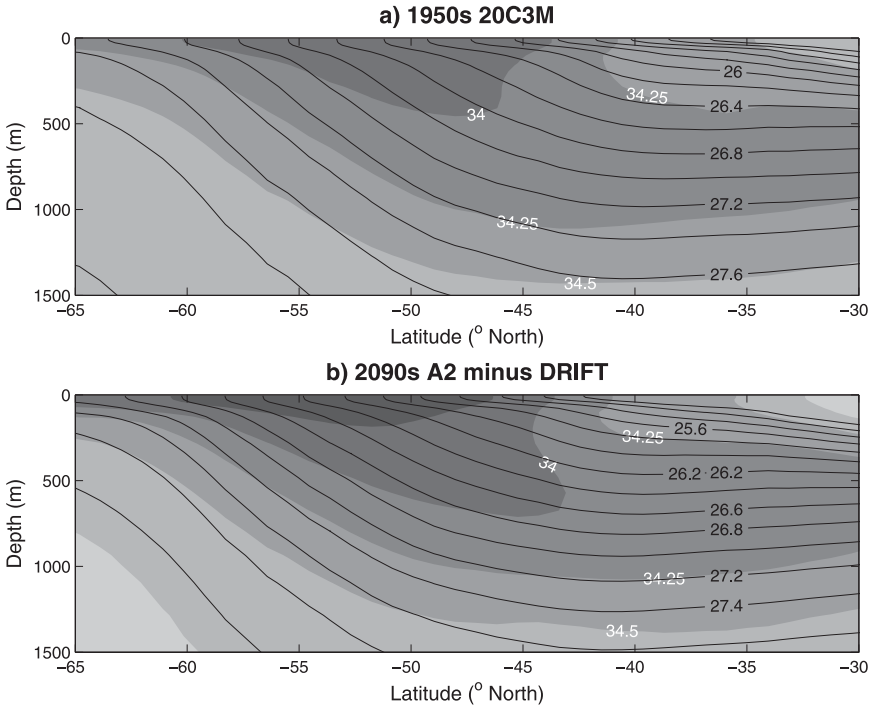

FIG. 2. Zonally averaged salinity (psu) with density surfaces (kg m^{-3}) overlaid for the (a) 1950s 20C3M and (b) 2090s A2 scenario with drift subtracted.

in the twentieth century in Sloyan and Kamenkovich (2007).

Changes in water mass properties on neutral density surfaces can vary because of changes occurring at the ocean surface (Bindoff and McDougall 1994). In the Southern Ocean, the ratio between temperature and salinity results in a θ–S curve with a positive slope, and hence a thermocline with a positive gradient. In this region, pure warming and pure freshening at the ocean's surface are both associated with cooling and freshening on density surfaces. However, as shown in Bindoff and McDougall (2000), if the slope of the thermocline is negative, the opposite effect would be observed: a warming signal on isobars (pure warming) would correspond with an increase in potential temperature and salinity on neutral surfaces.

c. Subduction estimation

The annual mean subduction rate reflects the seasonal evolution of the upper ocean: a decrease in the maximum winter mixed layer depth along the trajectory of a water column causes water masses to be permanently transferred into the ocean interior. A transfer from the mixed layer to the interior is defined as positive subduction. Between summer and autumn, the shallow mixed layer and heat input strengthen stratification. During autumn and early winter, fluid is entrained into the deepening winter mixed layer (MNW). The Gent and McWilliams (1990) isopycnal mixing scheme is included in the CSIRO Mk3.5; however, the contribution from each of the large-scale model velocities and the eddy-induced "bolus" transport are not calculated individually. We analyze decadal changes in the annual mean subduction rates based on the equations of MNW:

$$S_{\text{ann}} = -\mathbf{u}_H \cdot \nabla H - w_H, \tag{2}$$

where $\mathbf{u}_H \cdot \nabla H$ represents the component of the horizontal velocities perpendicular to the tilted base of the winter mixed layer depth, $z = -H$. The negative values that result from (2) correspond to zero subduction. The vertical velocity at the base of the mixed layer is calculated using the wind stress curl. This vertical term

TABLE 1. Density classes (kg m^{-3}) corresponding to SAMW and AAIW in the Indian, Pacific, and Atlantic Oceans during the 1950s and 2090s decadal periods.

Basin		1950s	2090s
Indian	SAMW	26.1–26.6	25.8–26.3
	AAIW	26.6–27.1	26.3–26.8
Pacific	SAMW	25.9–26.4	25.6–26.1
	AAIW	26.4–27.0	26.1–26.7
Atlantic	SAMW	26.0–26.6	25.9–26.5
	AAIW	26.6–27.2	26.5–27.1

includes the correction for the mixed layer meridional Sverdrup transport (Karstensen and Quadfasel 2002), which we found in the model to be strongest at the equator and at midlatitudes in the Southern Ocean, and is given by

$$w_H = \frac{1}{\rho}\left|\mathrm{curl}\left(\frac{\tau}{f}\right)\right| - \frac{\beta}{f}\int v dz. \quad (3)$$

The irreversible transfer of fluid into the ocean interior occurs over a short time scale in the Southern Ocean of only 1–2 months, hence we use the maximum winter mixed layer depth, H, in the calculation of the annual mean subduction rate.

d. Buoyancy contribution to subduction

We link the kinematic definition of subduction with the thermodynamics of the mixed layer and seasonal cycles to determine the variability in the relative contributions of surface fluxe s of heat and salt (freshwater) compared with the horizontal Ekman transport of heat and freshwater, both of which can alter the Southern Ocean circulation (MNW). The net surface buoyancy input (B_{net}; MNW) is given by

$$B_{\mathrm{net}} = \frac{g\alpha}{C_w} H_{\mathrm{in}} - g\beta\bar{\rho}S_m(E-P) - B_{\mathrm{Ek}}, \quad (4)$$

where a positive B_{net} indicates buoyancy gain (i.e., making the density of surface waters lighter) and a negative value indicates a buoyancy loss. The variable g is the gravitational force and the mean ocean density is given by $\bar{\rho}$. The first term in the above equation includes the surface heat flux (H_{in}), made up of latent and sensible heat and longwave and shortwave radiative fluxes; the thermal expansion coefficient (α); and the heat capacity of water (C_w). The second term represents the surface freshwater flux (evaporation, E, minus precipitation, P) with β the haline contraction coefficient and S_m the mixed layer salinity. Evaporation was calculated using latent heat (Q_{lat}), $E = Q_{\mathrm{lat}}/L$, where the latent heat of evaporation $L = 2.5 \times 10^6$ J kg^{-1}. The buoyancy amassed by the Ekman drift,

$$B_{\mathrm{Ek}} = \frac{g}{\bar{\rho}f}\mathbf{k} \times \boldsymbol{\tau} \cdot \nabla\rho_m, \quad (5)$$

is dependent on the curl of the wind stress. The unit vertical vector is represented by $\mathbf{k}$, and ρ_m is the averaged mixed layer density. We group the first two terms in (4) as air–sea fluxes, ASF $= (g\alpha/C_w)H_{\mathrm{in}} - g\beta\bar{\rho}S_m(E-P)$, and compare their contribution to changes in the net surface buoyancy flux with the Ekman fluxes of heat and freshwater, EkF $= -B_{\mathrm{Ek}}$.

3. Results

a. Water mass changes in the ocean interior

1) Decadal changes in water mass properties on γ^N

Variations in the temperature, salinity, and depth of neutral density surfaces were analyzed in the Southern Ocean for latitudes south of 32°S. The averaged $\theta-S$ plots (with drift subtracted from the projected 2090s A2 scenario) are shown in Fig. 3. In the model, SAMW exported from the Southern Ocean enters the subtropical gyres at depths between 200 and 600 dbar (where 1 dbar $\approx$ 1 m), with temperature and salinity properties ranging from 6° to 10°C and from 34.2 to 34.5 psu. In the 1950s, the model AAIW (3°–6°C; 33.9–34.2 psu) circulates at intermediate depths up to 900 dbar. AAIW is defined by its salinity minimum, found between 26.6 and 27.1 kg m^{-3} across the three basins. The changes in temperature and salinity have lightened densities over the entire water column, shown by the shift in the $\theta-S$ curves (Fig. 3). The model predicts cooling and freshening on neutral density surfaces in the 2090s across all three basins for densities lighter than 27.3 kg m^{-3}, and warmer and more saline waters are found at the Circumpolar Deep Water (CDW) densities, between approximately 27.3 and 28.0 kg m^{-3}. The importance of removing the model drift from the projected climate is emphasized for bottom water densities (>28.0 kg m^{-3}), where we found increases in the temperature and salinity for the 2090s A2 projection (figure not shown) but cooling and freshening after the drift is removed.

Freshening is projected to be strongest in the SAMW formation region in the Indian Ocean (Fig. 3a), averaging at 0.2 psu, using density classes in Table 1. There is smaller but significant freshening of about 0.1 psu in the mean Pacific and Atlantic basins in the 2090s (Figs. 3b,c), agreeing well with the late-twentieth-century observed pattern of change in SAMW (Aoki et al. 2005). The projected decreases in the salinity of AAIW are about half those of SAMW and mean basin freshening ranges from 0.06 to 0.1 psu. Even though cooling on density surfaces is apparent when comparing the same density ranges over time, the shift in the key water mass characteristics of mode and intermediate waters to lighter densities results in basin-averaged warming of between 0.9° and 1.5°C. Projected warming is strongest in the water mass formation regions and weakest in the west Pacific and subtropical Indian Oceans. The model increases in temperature for AAIW are greatest in the Indian and Pacific Oceans, in line with patterns observed in recent studies (Wong et al. 1999). The exception is cooling of 0.1°C of SAMW in the Atlantic Ocean during the 2090s.

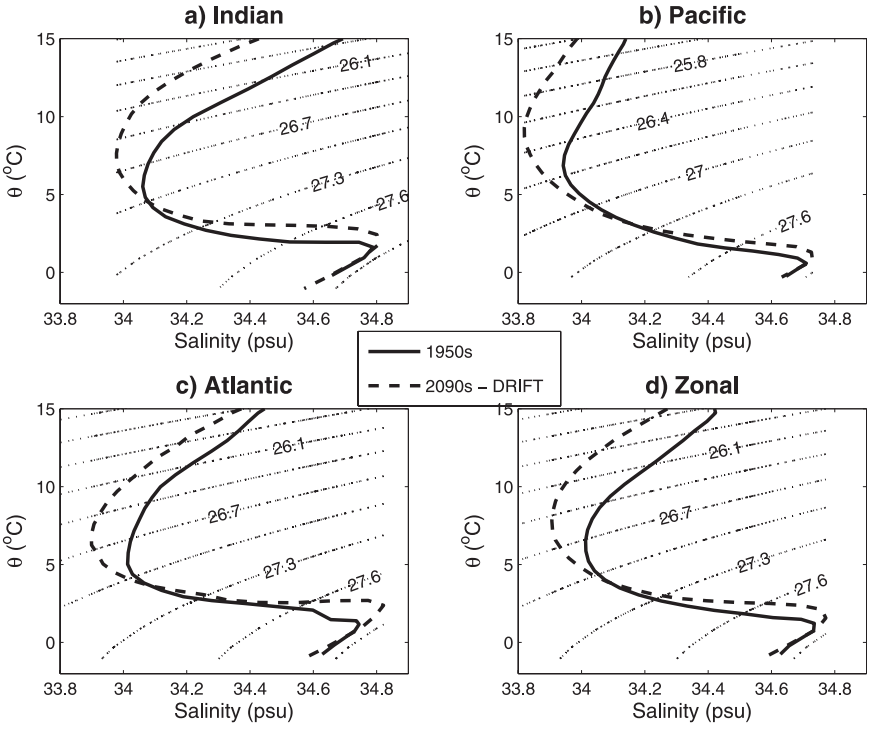

FIG. 3. Potential temperature (°C) vs salinity (psu) plots for the 1950s (solid) and 2090s A2 projection (dashed; model drift subtracted) averaged south of 32°S for the (a) Indian, (b) Pacific, and (c) Atlantic Oceans and (d) the zonal average. The dotted curves represent the combined 1950s and 2090s density surfaces in 0.3 kg m^{-3} intervals.

Changes in the depth of density surfaces occur because of either a horizontal meridional shift in the outcrop of the water mass or vertical displacement. An analysis of the zonally averaged meridional section of density surfaces in the 2090s (Fig. 4) shows projected deepening throughout the upper ocean, with the large changes near the outcrop regions due to a poleward shift of surface and underlying layers for densities greater than 25.5 kg m^{-3}. This deepening is greatest between 26.0 and 27.4 kg m^{-3} and is consistent across all three basins. The removal of the model drift from the A2 projection results in less deepening for densities lighter than 27.5 kg m^{-3} but more deepening for higher densities, particularly in deep water at low latitudes (figure not shown). We quantitatively assessed the features that define SAMW and AAIW masses (Table 1) and have found a large increase in depth (between 60 and 200 m) in the primary water mass formation regions, the southeast Indian and Pacific basins. North of these regions at subtropical latitudes, vertical displacement of density surfaces causes a shoaling pattern that is smaller in magnitude than in the outcrop regions.

Warming or freshening at the surface of the ocean in the SAMW formation region leads to cooling and freshening on neutral surfaces (Bindoff and McDougall 1994). Figure 5 displays the sea surface temperature differences (ΔSST) and salinity differences (ΔSSS) between the 1950s and 2090s decadal means. The simulation projects large-scale spatial changes, with surface warming spread throughout the Southern Ocean, excluding the Ross and Weddell Seas (Fig. 5a). Freshening is projected across mid- and high latitudes because of an increase in the precipitation rate and also a poleward shift in the precipitation band. More saline surface waters are projected in the tropics north of 35°S (Fig. 5b). The model projects warming between 1.5° and 3.5°C and freshening between 0.1 and 0.2 psu in the SAMW and AAIW formation zones. The modeled 2090s surface mode and intermediate water mass results are consistent with the pattern of temperature and salinity differences observed over the past 50 yr, such as the SST increase of between 0.3° and 1.0°C in the SAMW formation zone from 1962 to 1987 in Bindoff and McDougall (2000).

2) TRANSPORT ACROSS 32°S

Mode and intermediate water masses in the model are subducted and advected into the Southern Hemisphere subtropical gyres, and we now examine how the changes in the model water masses at the end of the twenty-first

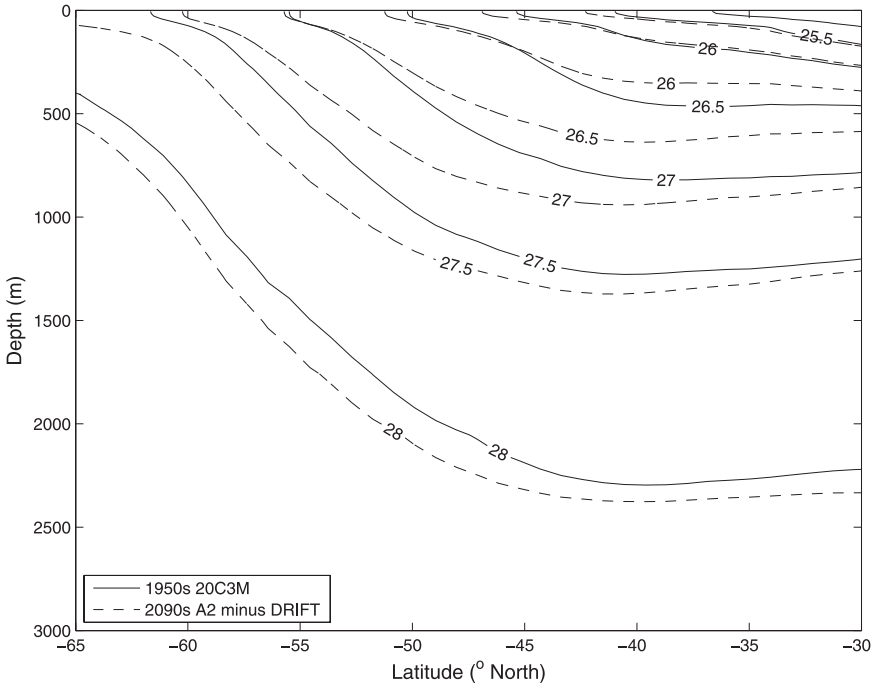

FIG. 4. Southern Ocean neutral density surfaces (kg m^{-3}) averaged zonally as a function of depth (m) for the decadal means 1950s (solid) and 2090s (dashed; model drift subtracted).

century are reflected as changes in the volume-transport inventory. We estimated the integrated volume transport across 32°S in each basin and also the zonal sum (Fig. 6), using this reference latitude so that our results can be compared with observations found along this transect. The transport values are calculated in density coordinates by using the decadal mean velocities. The 1950s model southward (9.6 Sv) and northward (2.8 Sv) transports across 32°S in the Indian and Pacific Oceans, respectively, are remarkably similar to the late twentieth century transports calculated from observations, between 26.0 and 27.4 kg m^{-3} (Sloyan and Rintoul 2001). The A2 projection shows a clear decrease in both poleward and equatorward transport at all densities, except in the upwelled CDW in the southern Indian and Pacific basins. Using the density classes in Table 1, we find the largest model changes in transport are in the Indian Ocean (Fig. 6a), where southward transport across 32°S decreases by approximately 40% (1.2 Sv for SAMW and 2 Sv for AAIW). Small decreases of less than 1 Sv in the northward transport of mode and intermediate water masses are projected in the Pacific and Atlantic Oceans (Figs. 6b,d), and a relatively large 0.7 Sv decrease (54%) in the northward transport of AAIW is predicted in the Atlantic Ocean. The only increase in transport in the 2090s occurs in the export of SAMW in the Atlantic basin (0.2 Sv), possibly related to the large increase in subduction of SAMW, discussed in the next section.

b. Subduction into the permanent thermocline

1) THE ANNUAL MEAN SUBDUCTION RATE

Using (2), we diagnosed the decadal average of the annual mean subduction rate over the 1950s. The strongest SAMW (AAIW) subduction rates are found north of (within) the zero wind stress curl, reaching over 100 m yr^{-1} (figure not shown). We converted the subduction rate to a volume transport through the mixed layer base and found that the 1950s estimates of subduction compare well with Karstensen and Quadfasel (2002) for densities lighter than 27.3 kg m^{-3} (the maximum density in their study). Karstensen and Quadfasel (2002) found the transport of fluid into the ocean interior via subduction to be 21, 35, and 44 Sv in the Atlantic, Indian, and Pacific Oceans, respectively. Our estimates of the volumes of fluid subducted in these basins, using the density ranges of Karstensen and Quadfasel (2002), were up to 30% higher in the Atlantic and Pacific basins but the same in the Indian Ocean. Differences from their study are due to our choice of mixed layer criterion [Karstensen and Quadfasel (2002) use $|\rho_m - \rho_s| \leq 0.125$ kg m^{-3}] and our inclusion of both the zonal and meridional components of the lateral subduction term [only $-v(dH/dy)$ is used for their study].

We analyzed the vertical ($-w_H$) and lateral ($-\mathbf{u}_H \cdot \nabla H$) contributions in (2) to the decadal mean subduction rate

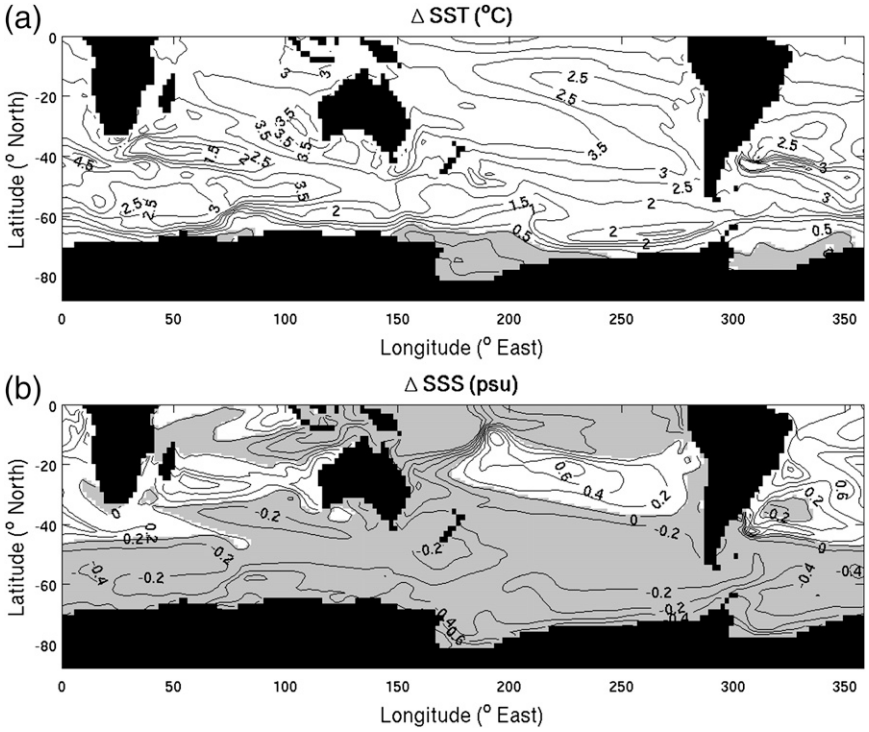

FIG. 5. Difference between 2090s and 1950s at the ocean surface for (a) temperature (°C) and (b) salinity (psu). Note that the model drift has been subtracted from the 2090s A2 projection. Negative values (i.e., decreases) are shaded.

(measured in Sverdrups) along density surfaces. SAMW and AAIW form close to the zero wind stress curl and this results in a small vertical subduction component. Hence, the model showed that the horizontal velocities perpendicular to the mixed layer tilt contributed to most of the annual mean subduction of SAMW and AAIW in the 1950s (Fig. 7). The exception is in the Atlantic Ocean (Fig. 7c), where the vertical and lateral components contribute equally for densities lighter than 25.8 kg m^{-3}. However, Huang and Qiu (1998) found that of the 21.6 Sv of water masses ventilated in the South Pacific, only 3.5 Sv were attributed to the lateral term, which could be a result of smoothing of climatology for densities greater than 27.0 kg m^{-3} in the Southern Ocean and an inaccurate representation of the winter mixed layer depth.

The projected changes in subduction are assessed in this study using basin means, because there is significant zonal variation in the spatial pattern, particularly because of the strong gradients in the lateral induction term. The 1950s model SAMW volume of fluid subducted is 10.0, 9.5, and a small 2.9 Sv in the Indian, Pacific, and Atlantic Oceans, respectively. There is a large volume of 26.2 Sv of AAIW subducted in the Pacific Ocean and volumes of 6.5 and 6.0 Sv are subducted in the Indian and Atlantic basins, respectively. Using the density classes in Table 1, we deduced the changes in the annual mean subduction rates for SAMW and AAIW in the 2090s (Fig. 8). The combined and projected decreases of 2.1 and 2.3 Sv in the subduction of SAMW in the Indian and Pacific Oceans, respectively (Figs. 8a,b) balance the 4.6 Sv increase in the Atlantic basin (Fig. 8c). This implies that the volume of fluid subducted for SAMW does not change; rather, the water mass moves to a lighter density class. However, there are significant decreases in the 2090s subduction of AAIW (3.9, 12.3, and 3.6 Sv in the Indian, Atlantic, and Pacific Oceans, respectively), as well as a decrease in its outcrop density. The projected decreases in the subduction of SAMW and AAIW are dominated by decreases in the lateral term ($-\mathbf{u}_H \cdot \nabla H$) because of the winter mixed layer shoaling by 200 and 150 m in the SAMW and AAIW formation regions, respectively.

2) THE ROLE OF BUOYANCY

The influence of air–sea fluxes from continents during winter is weaker over the Southern Ocean compared with the Northern Hemisphere. An ocean heat gain occurs as the cold UCDW is transported equatorward in the Ekman layer (associated with B_{Ek} negative) across

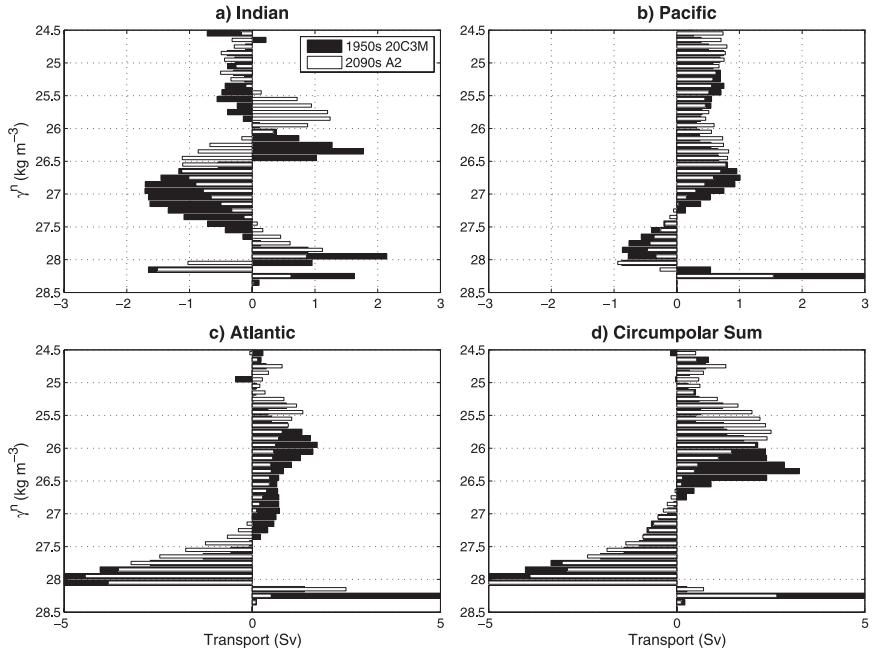

FIG. 6. Northward volume transport (Sv) across 32°S for the 1950s (black) and 2090s (white) decadal periods in the (a) Indian, (b) Pacific, (c) and Atlantic Oceans and (d) the circumpolar sum.

the ACC toward the equator (Speer et al. 2000). The water converges in the deep mixed layers north of the ACC, where mode and intermediate water masses are formed. A loss of heat through winter cooling results in buoyancy lost to the atmosphere (B_{in} negative), which drives the mixing that deepens the mixed layers in the southeast Indian and Pacific basins. The 1950s model net surface buoyancy flux for the SAMW and AAIW formation regions ranges between 2×10^{-6} and 13×10^{-6} kg m^{-1} s^{-3}, which is slightly greater than observations (Zhang and Talley 1998; Karstensen and Quadfasel 2002). The loss of buoyancy resulting from winter cooling exceeded the buoyancy gain supplied over the warmer months, and the heat transferred through the Ekman flux was found to be main driver during both decadal periods.

The net surface buoyancy flux [Eq. (4)] has shifted toward lighter densities over the 150-yr period, and its change in terms of the surface density is shown in Fig. 9. In density space, the zonally averaged decrease in the annual mean loss of the net surface buoyancy flux (B_{net}) is dominated by the increase in the heat and freshwater driven by the Ekman flux for densities greater than 26.6 kg m^{-3} (mainly due to increases in the freshwater component). For densities less than 26.6 kg m^{-3}, the surface heat flux in the Indian Ocean (Fig. 9a) and the heat transported in the Ekman layer in the Pacific Ocean (Fig. 9b) result in a decrease in the net surface buoyancy flux. In the Atlantic basin (Fig. 9c), the overall decrease in the 1950s B_{net} loss (shown as positive values) is strongly governed by the increases in the ASF term.

Under increasing CO_2 forcing, Banks et al. (2002) concluded that changes in SAMW properties along isopycnals in the Indian Ocean were caused by surface heating, with a smaller contribution from freshwater fluxes. Similarly, we find that the projected increases in the heat transported through the Ekman flux dominate the increase in the loss of the SAMW net surface buoyancy flux. The projected 2×10^{-6} kg m^{-1} s^{-3} increase in the SAMW buoyancy flux in the Indian Ocean is balanced by the combined smaller decreases in the Pacific and Atlantic Oceans, resulting in a negligible zonal mean change. The model increase in the surface freshwater flux drives a decrease in the (negative) AAIW net surface buoyancy flux in all three basins, and there is a maximum basin-average decrease in the total air–sea fluxes of 5×10^{-6} kg m^{-1} s^{-3} found for AAIW densities in the Pacific Ocean. These AAIW buoyancy flux decreases are dominated by increases in the surface heat and freshwater fluxes (ASF), even though the Ekman-transported fluxes (EkF) dominate the net buoyancy flux in each of the decadal periods. The projected decreases in the AAIW net surface buoyancy flux mimic those of the subduction rate, implying a direct relationship between subduction (see Fig. 8) and buoyancy, as discussed in MNW.

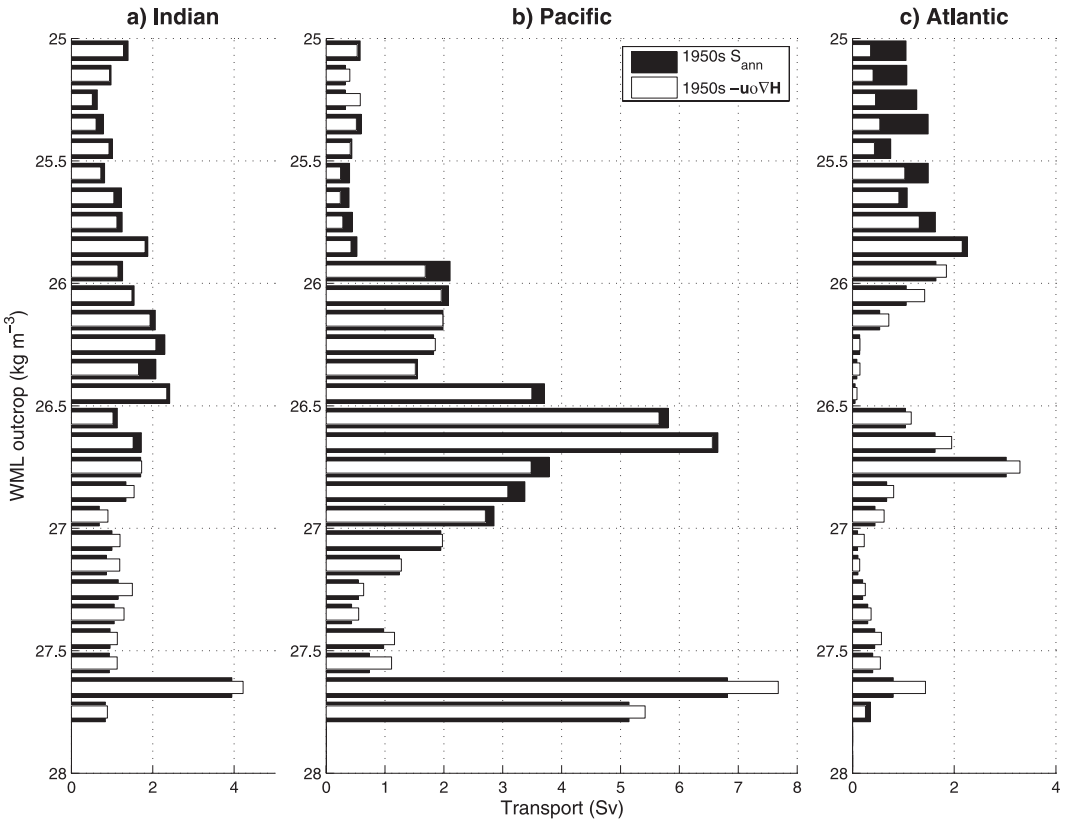

FIG. 7. Zonally averaged 1950s $\boldsymbol{S}_{\text{ann}}$ (Sv; black) with northward lateral component ($-\mathbf{u}_H \cdot \nabla H$; white) plotted against the WML outcrop in 0.1 kg m^{-3} density bins for the (a) Indian, (b) Pacific, and (c) Atlantic Oceans.

4. Discussion and conclusions

We have compared the 1950s and 2090s decadal mean climate variables to diagnose the future changes in SAMW and AAIW water mass properties in the Southern Ocean, using the CSIRO Mk3.5 climate system model. We assessed changes in SAMW and AAIW quantitatively using Table 1, noting that the water masses were associated with a different density range in each basin because of varying temperature and salinity signatures and subduction rates. Model drift [Eq. (1)] was removed from the A2 scenario for variables associated with temperature and salinity. An analysis of the subduction of SAMW and AAIW was also performed using the earlier CSIRO Mk3.0 model, and we drew similar conclusions with regard to subduction changes in a future climate scenario. However, a range of biases in the CSIRO Mk3.0 model (Sloyan and Kamenkovich 2007) resulted in unrealistically large subduction rates during the twentieth century, making this model version an inferior choice for assessing future changes in the ventilation of SAMW and AAIW.

The model projects cooling and freshening for density surfaces lighter than 27.3 kg m^{-3}, and SAMW and AAIW warm and shift to lighter densities. Both water masses show freshening of up to 0.2 psu, associated with warming and freshening at the ocean surface. Bindoff and McDougall (2000) noted that the salinity minimum at the source of AAIW in the southeast Pacific has freshened via an increased freshwater flux, and we find this to be the case in the A2 climate projection with freshening of 0.1 psu. The projected pattern of water mass change in the model is strikingly similar to the observed changes over the much shorter period from the 1960s to 2001 (Wong et al. 1999; Bindoff and McDougall 2000; Aoki et al. 2005).

The potential vorticity at the base of the mixed layer increases (indicating stronger stratification) from approximately 3.5×10^{-10} to 5×10^{-10} m^{-1} s^{-1} when averaged over the density classes (Table 1) of both SAMW and AAIW water masses, and this is associated with the overall projected decrease in the net surface buoyancy flux. In both the 1950s and 2090s, the mean loss of the buoyancy flux is governed by the mean northward Ekman transport of cold, fresh fluid into the SAMW and AAIW formation regions, in agreement with Rintoul and England (2002). Banks and Bindoff

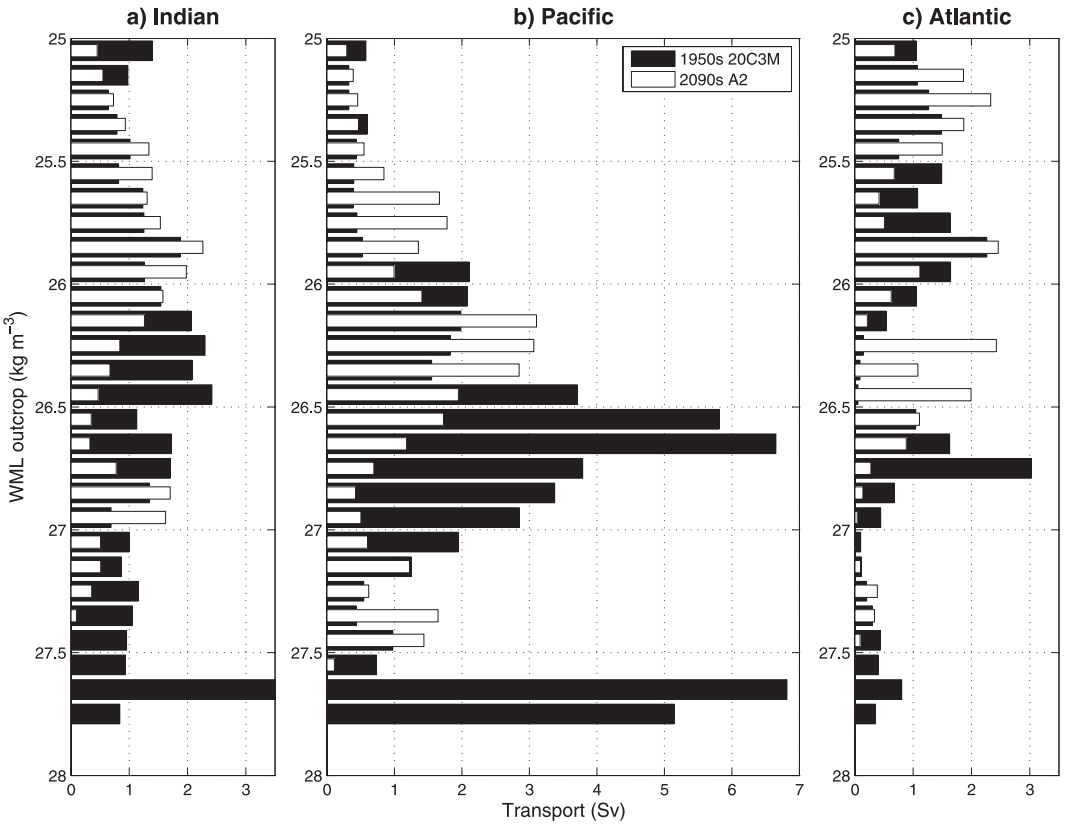

FIG. 8. Zonally averaged 1950s $\boldsymbol{S}_{\text{ann}}$ (Sv; black) and the 2090s A2 projection (white), plotted against the WML outcrop density (kg m^{-3}) for the (a) Indian, (b) Pacific, and (c) Atlantic Oceans.

(2003) found modeled and observed changes in surface heat fluxes drove variations in mode and intermediate water masses for the last 40 yr. Our study indicated that although the buoyancy losses in the decadal mean climate were driven by Ekman fluxes, the changes in the surface heat and freshwater fluxes were the strongest factors in decreasing the buoyancy loss. This follows the Murray et al. (2007) study, which concluded that the wind stress dominated SAMW formation over a shorter term but played a minor role in the perturbation to the mean climate over decadal time scales. The exception was in the Indian Ocean (Fig. 9a) at SAMW densities, where projected strengthening of the westerlies shifting to lighter densities dominates the modeled increase in the loss of the 1950s net surface buoyancy flux.

We find that the lateral term at the base of the winter mixed layer ($-\mathbf{u}_H \cdot \nabla H$) dominates the model subduction of SAMW and AAIW during both decadal periods, with little input from the vertical term ($-w_H$). The projected decrease in the winter mixed layer depth (up to 200 m) was responsible for a decrease in the subduction of AAIW by a maximum of 12.3 Sv (Pacific Ocean). A balance between the decreases in the subduction of SAMW in the Indian and Pacific Oceans and an increase in the Atlantic Ocean result in negligible net change. Except for the small projected increase in the export of SAMW in the Atlantic Ocean (0.2 Sv), the volume transport across 32°S on density surfaces decreases in all three basins for mode and intermediate water masses, with the greatest reduction being 2.0 Sv in the southward transport of AAIW in the Indian Ocean. The modeled deepening of density surfaces at the outcrop regions is due to southward displacement, and vertical heaving was responsible for the smaller amounts of deepening of density surfaces in the subtropics (Fig. 4). We found the pattern of the projected changes in the volume of fluid subducted and the volume transport across 32°S to be similar; however, the magnitudes of changes in subduction were greater.

We see that a projected combination of the decreases in the negative net surface buoyancy flux, the stronger potential vorticity at the base of the mixed layer, the decreases in the winter mixed layer, and warming and freshening at the surface cause an overall decrease in the subduction of AAIW into the ocean's interior between the 1950s and 2090s, with little change in the total subduction of SAMW. The Southern Ocean absorbs atmospheric CO_2 and the subduction of SAMW and

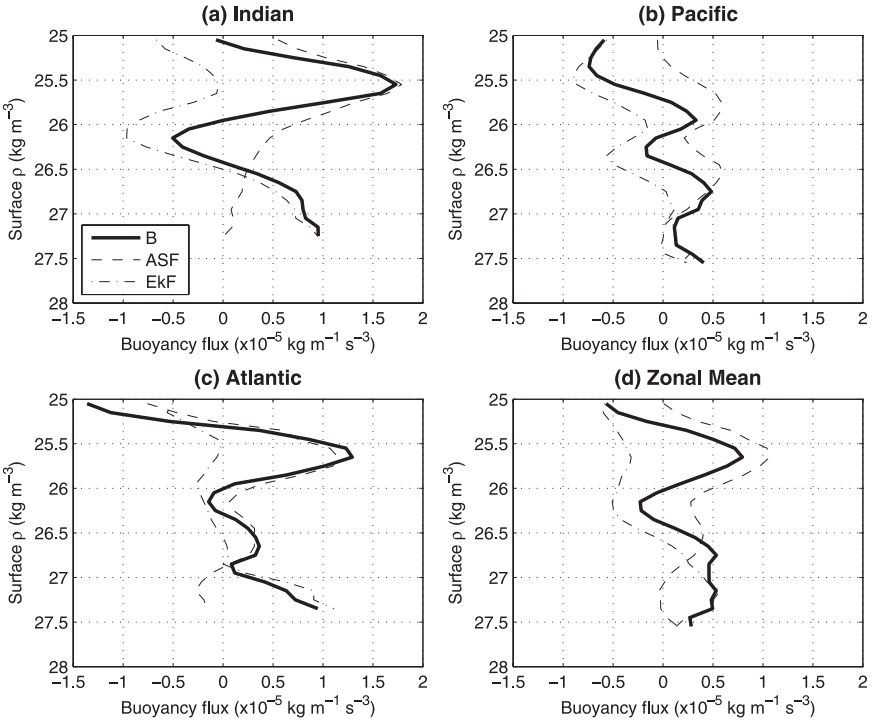

FIG. 9. Difference (2090s minus 1950s) in the Southern Ocean net surface buoyancy flux ($\times 10^{-5}$ kg m^{-1} s^{-3}) in the (a) Indian, (b) Pacific, and (c) Atlantic Oceans and (d) the zonal mean. Also shown is the difference in each of the two buoyancy components from Eqs. (4) and (5): the ASF (dashed) and the EkF (dotted–dashed). Positive values indicate a net buoyancy gain (i.e., lighter density), and negative values indicate a buoyancy loss.

AAIW carries a significant amount of the anthropogenic CO_2 into the ocean's interior in the present-day climate. An overall decrease in the subduction of the water masses in the upper-limb Southern Ocean overturning circulation suggests the capacity of the Southern Ocean to absorb CO_2 is likely to decrease in the future.

Acknowledgments. This work is supported by the Australian Government's Cooperative Research Centres Programme through the Antarctic Climate and Ecosystems CRC, the CSIRO Wealth from Oceans National Flagship, and the Australian Climate Change Science Program. We greatly appreciate the discussions on the theory of neutral surfaces with Trevor McDougall and David Jackett, and we would like to express our thanks to Glenn Hyland and Martin Dix for their assistance with access to data. We acknowledge the modeling groups for providing their data for analysis, the Program for Climate Model Diagnosis and Intercomparison (PCMDI) for collecting and archiving the model output, and the JSC/CLIVAR Working Group on Coupled Modelling (WGCM) for organizing the model data analysis activity. The multimodel data archive is supported by the Office of Science, U.S. Department of Energy.

REFERENCES

Aoki, S., M. Yoritaka, and A. Masuyama, 2003: Multidecadal warming of subsurface temperature in the Indian sector of the Southern Ocean. *J. Geophys. Res.,* **108,** 8081, doi:10.1029/2000JC000307.

——, N. L. Bindoff, and J. A. Church, 2005: Interdecadal water mass changes in the Southern Ocean between 30°E and 160°E. *Geophys. Res. Lett.,* **32,** L07607, doi:10.1029/2004GL022220.

Banks, H. T., and N. L. Bindoff, 2003: Comparison of observed temperature and salinity changes in the Indo-Pacific with results from the coupled climate model HadCM3: Processes and mechanisms. *J. Climate,* **16,** 156–166.

——, R. Wood, and J. Gregory, 2002: Changes to Indian Ocean subantarctic mode water in a coupled climate model as CO_2 forcing increases. *J. Phys. Oceanogr.,* **32,** 2816–2827.

Bindoff, N. L., and T. J. McDougall, 1994: Diagnosing climate change and ocean ventilation using hydrographic data. *J. Phys. Oceanogr.,* **24,** 1137–1152.

——, and ——, 2000: Decadal changes along an Indian Ocean section at 32°S and their interpretation. *J. Phys. Oceanogr.,* **30,** 1207–1222.

Bryden, H. L., E. L. McDonagh, and B. A. King, 2003: Changes in ocean water mass properties: Oscillations or trends? *Science,* **300,** 2086–2088.

Cunningham, S. A., S. G. Alderson, B. A. King, and M. A. Brandon, 2003: Transport and variability of the Antarctic Circumpolar Current in Drake Passage. *J. Geophys. Res.,* **108,** 8084, doi:10.1029/2001JC001147.

Curry, R., B. Dickson, and I. Yashayaev, 2003: A change in the freshwater balance of the Atlantic Ocean over the past four decades. *Nature,* **426,** 826–829.

de Boyer Montégut, C., G. Madec, A. S. Fischer, A. Lazar, and D. Iudicone, 2004: Mixed layer depth over the global ocean: An examination of profile data and a profile-based climatology. *J. Geophys. Res.,* **109,** C12003, doi:10.1029/2004JC002378.

Drijfhout, S. S., J. Donners, and W. P. M. de Ruijter, 2005: The origin of intermediate and subpolar mode waters crossing the Atlantic equator in OCCAM. *Geophys. Res. Lett.,* **32,** L06602, doi:10.1029/2004GL021851.

Fine, R. A., W. M. Smethie Jr., J. L. Bullister, M. Rhein, D.-H. Min, M. J. Warner, A. Poisson, and R. F. Weiss, 2008: Decadal ventilation and mixing of Indian Ocean waters. *Deep-Sea Res. I,* **55,** 20–37.

Gent, P. R., and J. C. McWilliams, 1990: Isopycnal mixing in ocean circulation models. *J. Phys. Oceanogr.,* **20,** 150–155.

Gille, S. T., 2002: Warming of the Southern Ocean since the 1950s. *Science,* **295,** 1275–1277.

Goes, M., I. Wainier, P. R. Gent, and F. O. Bryan, 2008: Changes in subduction in the South Atlantic Ocean during the 21st century in the CCSM3. *J. Geophys. Res.,* **35,** L06701, doi:10.1029/2007GL032762.

Gordon, H. B., and Coauthors, 2002: The CSIRO Mk3 climate system model. CSIRO Atmospheric Research Tech. Rep. 60, 134 pp.

Huang, R. X., and B. Qiu, 1998: The structure of the wind-driven circulation in the subtropical South Pacific Ocean. *J. Phys. Oceanogr.,* **28,** 1173–1186.

Jackett, D. R., and T. J. McDougall, 1997: A neutral density variable for the world's oceans. *J. Phys. Oceanogr.,* **27,** 237–263.

Johnson, G. C., and A. H. Orsi, 1997: Southwest Pacific Ocean water-mass changes between 1968/69 and 1990/91. *J. Climate,* **10,** 306–316.

Karstensen, J., 2004: Formation of South Pacific shallow salinity minimum: A Southern Ocean pathway to the tropical Pacific. *J. Phys. Oceanogr.,* **34,** 2398–2412.

——, and D. Quadfasel, 2002: Formation of Southern Hemisphere thermocline waters: Water mass conversion and subduction. *J. Phys. Oceanogr.,* **32,** 3020–3038.

Leonard, B. P., 1979: A stable and accurate convective modelling procedure based on quadratic upstream interpolation. *Comput. Methods Appl. Mech. Eng.,* **19,** 59–98.

Marshall, J. C., R. G. Williams, and A. J. G. Nurser, 1993: Inferring the subduction rate and period over the North Atlantic. *J. Phys. Oceanogr.,* **23,** 1315–1329.

Murray, R. J., N. L. Bindoff, and C. J. C. Reason, 2007: Modeling decadal changes on the Indian Ocean section I5 at 32°S. *J. Climate,* **20,** 3106–3130.

Orsi, A. H., and T. Whitworth III, 2007: *Southern Ocean.* Vol. 1, *Hydrographic Atlas of the World Ocean Circulation Experiment (WOCE)*. International WOCE Project Office.

Pacanowski, R. C., 1996: MOM 2 version 2, documentation, user's guide and reference manual. GFDL Ocean Tech. Rep. 3.2, 329 pp.

Rintoul, S. R., and M. H. England, 2002: Ekman transport dominates local air–sea fluxes in driving variability of Subantarctic Mode Water. *J. Phys. Oceanogr.,* **32,** 1308–1321.

Sabine, C. L., R. M. Key, K. M. Johnson, F. J. Millero, A. Poisson, J. L. Sarmiento, D. W. R. Wallace, and C. D. Winn, 1999: Anthropogenic CO_2 inventory of the Indian Ocean. *Global Biogeochem. Cycles,* **13,** 179–198.

——, and Coauthors, 2004: The oceanic sink for anthropogenic CO_2. *Science,* **305,** 367–371.

Sallée, J.-B., N. Wienders, K. Speer, and R. Morrow, 2006: Formation of subantarctic mode water in the southeastern Indian Ocean. *Ocean Dyn.,* **56,** 525–542.

Santoso, A., and M. H. England, 2004: Antarctic Intermediate Water circulation and variability in a coupled clime model. *J. Phys. Oceanogr.,* **34,** 2160–2179.

Sarmiento, J. L., T. M. C. Hughes, R. J. Stouffer, and S. Manabe, 1998: Simulated response of the ocean carbon cycle to anthropogenic climate warming. *Nature,* **393,** 245–249.

Sloyan, B. M., and S. R. Rintoul, 2001: The Southern Ocean limb of the global deep overturning circulation. *J. Phys. Oceanogr.,* **31,** 143–173.

——, and I. V. Kamenkovich, 2007: Simulation of subantarctic mode water and Antarctic Intermediate Water in climate models. *J. Climate,* **20,** 5061–5080.

Spall, M., R. Weller, and P. Furey, 2000: Modeling the three-dimensional upper ocean heat budget and subduction rate during the Subduction Experiment. *J. Geophys. Res.,* **105** (C11), 26 151–26 166.

Speer, K., S. R. Rintoul, and B. Sloyan, 2000: The diabatic deacon cell. *J. Phys. Oceanogr.,* **30,** 3212–3222.

Talley, L. D., 2007: *Pacific Ocean.* Vol. 2, *Hydrographic Atlas of the World Ocean Circulation Experiment (WOCE)*. International WOCE Project Office.

Visbeck, M., J. Marshall, T. Haine, and M. Spall, 1997: Specification of eddy transfer coefficients in coarse-resolution ocean circulation models. *J. Phys. Oceanogr.,* **27,** 381–402.

Wong, A. P. S., N. L. Bindoff, and J. A. Church, 1999: Large-scale freshening of intermediate waters in the Pacific and Indian oceans. *Nature,* **400,** 440–443.

Zhang, H.-M., and L. D. Talley, 1998: Heat and buoyancy budgets and mixing rates in the upper thermocline of the Indian and Global Oceans. *J. Phys. Oceanogr.,* **28,** 1961–1978.